Dyes and Pigments 188 (2021) 109180

Contents lists available at ScienceDirect

Dyes and Pigments

journal homepage: http://www.elsevier.com/locate/dyepig

A novel endoplasmic reticulum-targeted ratiometric fluorescent probe based on FRET for the detection of SO_2 derivatives

Zhang-Yi Li [a], Xiao-Ling Cui [b], Ye-Hao Yan [a], Qiao-Ling Che [a], Jun-Ying Miao [b], Bao-Xiang Zhao [a,*], Zhao-Min Lin [c,**]

[a] Institute of Organic Chemistry, School of Chemistry and Chemical Engineering, Shandong University, Jinan, 250100, PR China
[b] Shandong Provincial Key Laboratory of Animal Cells and Developmental Biology, School of Life Science, Shandong University, Qingdao, 266237, PR China
[c] Institute of Medical Science, The Second Hospital of Shandong University, Jinan, 250033, PR China

ARTICLE INFO

Keywords:
Ratiometric fluorescence probe
FRET
SO_2 derivatives
Cell image
ER-Targeted

ABSTRACT

A novel FRET-based fluorescence probe, **NBIS**, constructed by benzoindole-based hemicyanine as an acceptor and naphthalimide derivatives as a donor was developed for the detecting of sulfur dioxide (SO_2) derivatives. Probe **NBIS** exhibited high energy transfer efficiency (89%) and showed high sensitivity (LOD: 16.2 nM) toward HSO_3^-/SO_3^{2-}. Probe **NBIS** could target the endoplasmic reticulum (ER) and was applied to image exogenous and endogenous HSO_3^-/SO_3^{2-} in living cells.

1. Introduction

It is known that continuous exposure to air pollution, in which sulfur dioxide (SO_2) is a main composition, might enhance chance of suffering cardiovascular and lung diseases. On the other hand, SO_2 derivatives are among the most widely utilized preservatives in the food and beverages industries, such as winemaking, and one of their main functions is to inhibit microorganisms. Under physiological conditions, SO_2 can dissolve in water and form its derivatives, bisulfite and sulfite [1,2]. There are many analytical methods for the assay of SO_2 preserving agents including titrimetric, spectrometric, chromatographic, electrochemical (voltammetric, amperometric, potentiometric) [3]. To date, the endogenous nature and possible physiological roles of SO_2 has gained attention. There is mounting evidence that SO_2 can be generated during normal cellular metabolism and may possibly function as a signaling molecule in normal physiology. For example, a complete endogenous SO_2 pathway was detected in the cardiovascular system and found to play an important role in cardiovascular physiology and pathophysiology [4]. Endogenous SO_2 could regulate hippocampal neuron apoptosis in developing epileptic rats [5]. Therefore, it is important to develop methods for detecting exogenous and endogenous SO_2 (HSO_3^-/SO_3^{2-}). Compared with traditional detection methods, fluorescent probe assay is more practical because of excellent advantages such as low cost, rapidity, high selectivity and sensitivity, non-invasive detection, good bio-compatibility as well as real-time detectability. In the last decade, fluorescent probes for the detection of SO_2 derivatives have been developed rapidly. Many fluorescent probes based on different sensing mechanisms including Michael addition, deprotection reaction, nucleophilic reaction with aldehyde have been designed and used to the detection of SO_2 derivatives [6–8]. Fluorescent probes typically fall into two categories, those which rely upon a single emission signal and those which employ a ratiometric. Because ratiometric fluorescence probes that allow measurement of the fluorescence emission intensities at two different wavelengths can eliminate interference from, for example, environmental effects, and the concentration of the probe by self-calibration, ratiometric fluorescence probes are highly desirable. So far, a number of ratiometric fluorescence probes based on different response mechanism, such as the intramolecular charge transfer (ICT), photoinduced electron transfer (PET), excited-state intramolecular proton transfer (ESIPT), through bond energy transfer (TBET) and fluorescence resonance energy transfer (FRET) have been reported to sense a wide variety of analytes, such as pH [9–11], HSO_3^- [12–19], peroxynitrite [20], thiol [21–23], hypochlorite [24,25], Fe^{3+} [26], Ca^{2+} [27], β-Galactosidase [28], hydrogen sulfide (H_2S) [29,30], Among them, FRET-based ratiometric fluorescence probes are very popular [31–37]. However, some deficiencies require

* Corresponding author.
** Corresponding author.
E-mail addresses: bxzhao@sdu.edu.cn (B.-X. Zhao), linzhaomin@sdu.edu.cn (Z.-M. Lin).

https://doi.org/10.1016/j.dyepig.2021.109180
Received 12 December 2020; Received in revised form 21 January 2021; Accepted 21 January 2021
Available online 30 January 2021

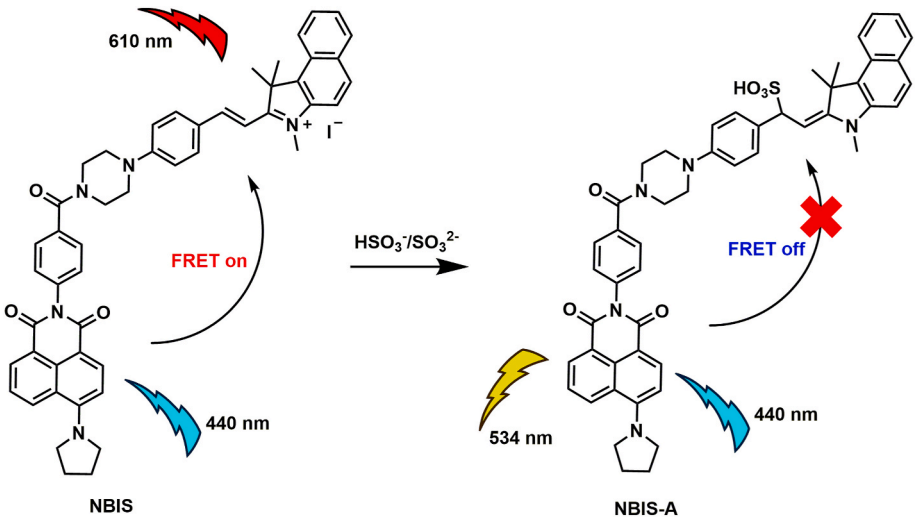

Scheme 1. Sensing mechanism of probe **NBIS** toward HSO_3^-/SO_3^{2-}

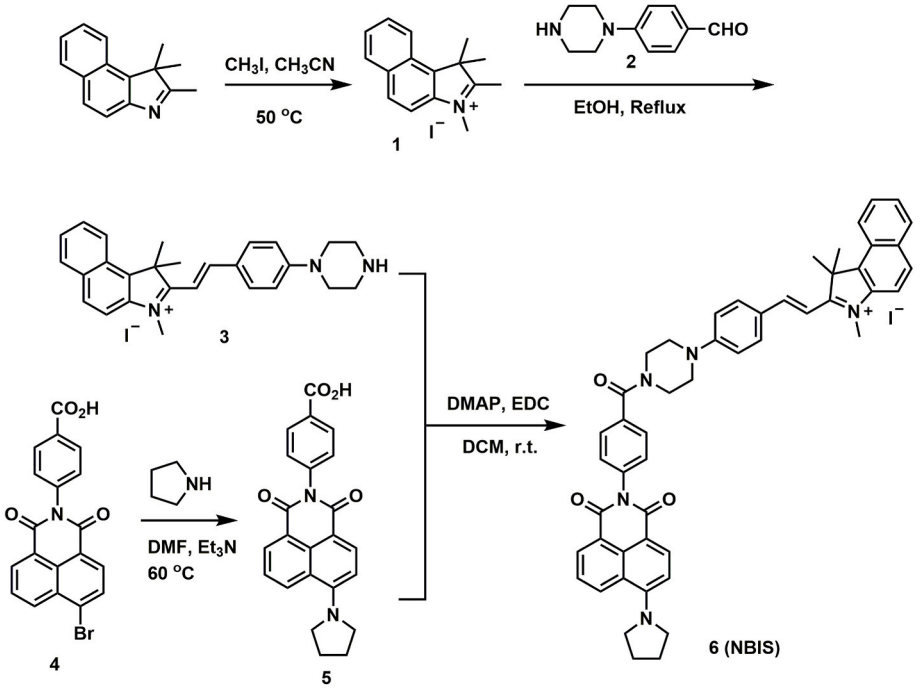

Scheme 2. Synthesis of probe **NBIS**.

improvement, such as response time, sensitivity, energy transfer efficiency [38], the distance between two emission bands [39], excitation wavelength [40]. Therefore, it is imperative to develop new FRET platforms. Notably, over the past decade, the design and development of organelle-targeted fluorescent probes have been attractive for precise monitoring of subcellular microenvironments. Though many probes with diverse targeting groups have been used to detect bioactive species, such as reactive oxygen species, reactive nitrogen species, reactive sulfur species, in specific organelles, endoplasmic reticulum (ER)-targeted fluorescence probes are very rare and the ER-targeted intrinsic molecular mechanism remains unclear [41]. To the best of our knowledge, ER-targeted fluorescent probe for monitoring of SO_2 derivatives has not been reported yet.

As a continuation of our efforts to develop new fluorescent probes, herein, we report a novel ER-targeted ratiometric fluorescent probe based on FRET for the detecting of SO_2 derivatives (Scheme 1).

2. Experimental section

2.1. Apparatus and material

^{1}H NMR and ^{13}C NMR spectra were determined by Bruker Avance 300 spectrometer. Mass spectra were recorded by a Q-TOF6510 spectrograph (Agilent). IR spectra were obtained using IR spectrophotometer VERTEX 70 FT-IR (Bruker Optics). UV–Vis absorption spectra were obtained by a Cary 5000 spectrophotometer (Agilent) and fluorescence spectra were measured on a LS-55 fluorescence spectrophotometer (PerkinElmer). The fluorescence lifetime was performed on an Edinburgh Instruments FLS920 Fluorescence Spectrometer. All pH of solutions were obtained by a PHS-3C pH-meter (YouKe). Thin-layer chromatography (TLC) was conducted on silica gel 60F_{254} plates (Merck KGaA) and column chromatography was carried out over silica gel (200–300 mesh). Unless otherwise stated, all reagents and solvents were

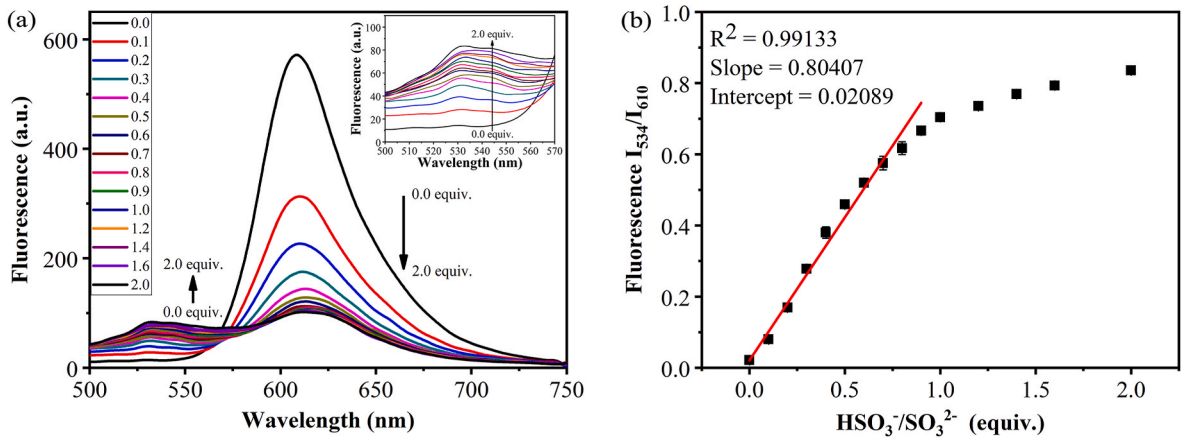

Fig. 1. (a) Probe **NBIS** (5 μM) responded toward HSO_3^-/SO_3^{2-} (0–2.0 equiv.). (b) The linear relationship between the ratio values of fluorescence intensity (I_{534}/I_{610}). Data are mean ± SD (n = 3). λ_{ex} = 440 nm, slit: 7.5/7.5 nm, speed: 1200 nm/min.

purchased from commercial provider. Twice-distilled water was used throughout all experiments.

2.2. Synthesis of probe *NBIS*

As shown in Scheme 2, the mixture of compound **3** (523 mg, 1.0 mmol), compound **5** (387 mg, 1.0 mmol), 4-dimethylaminopyridine (15 mg, 0.12 mmol) and 1-(3-dimethylaminopropyl)-3-ethylcarbodiimide hydrochloride (191 mg, 1.0 mmol) in dichloromethane (140 mL) was stirred at room temperature for 18 h. The solvent was removed under reduced pressure and then the residue was purified by column chromatography on silica gel to obtain probe **NBIS** (408 mg, dark violet solid) in 46% yield, which was characterized by NMR, HRMS and IR (Figs. S1–4). m. p. = 224–226 °C. ^{1}H NMR (300 MHz, $CDCl_3$) δ 8.66 (d, *J* = 8.4 Hz, 1H), 8.59–8.57 (m, 1H), 8.45–8.41 (m, 1H), 8.26–8.17 (m, 4H), 8.08–8.01 (m, 2H), 7.73–7.68 (m, 2H), 7.63–7.54 (m, 5H), 7.42–7.39 (m, 2H), 6.97 (d, *J* = 3.9 Hz, 2H), 6.86–6.83 (m, 1H), 4.42 (d, *J* = 4.5 Hz, 3H), 3.82–3.73 (m, 8H), 3.56–3.48 (m, 4H), 2.13 (m, 4H), 2.07 (s, 6H). ^{13}CNMR (75 MHz, DMSO-d_6) δ 181.72, 169.30, 164.45, 163.42, 154.35, 153.08, 152.94, 140.03, 138.17, 137.18, 135.60, 133.98, 133.47, 133.17, 131.59, 131.22, 131.10, 130.46, 129.92, 128.69, 128.06, 127.28, 126.97, 124.39, 123.71, 123.31, 122.37, 114.16, 113.33, 109.42, 108.99, 107.10, 56.49, 55.37, 53.40, 53.37, 46.62, 34.50, 26.26, 26.04, 19.01. IR (KBr, cm^{-1}): 3443, 2925, 2858, 1637, 1577, 1523, 1458, 1398, 1361, 1299, 1238, 1183, 1124, 1087. HRMS (ESI): *m/z* found 764.3530, calculated for $[C_{50}H_{46}O_3N_5]^+$: 764.3595.

2.3. Preparation of testing solution and cells culturing

A stock solution of probe **NBIS** (1 mM) was prepared in DMSO. The stock solutions of other analytes were prepared by using distilled water. 50 μL stock solution of probe **NBIS** was transferred into volumetric flask and diluted to 10 mL by the buffer solution (DMSO:PBS = 3:7, v/v, pH = 7.4) at room temperature. Then, various equivalents of HSO_3^-/SO_3^{2-} or other analytes was added.

Henrietta Lacks cells (HeLa cells), human liver cancer cells (HepG2 cells), human normal liver cells (L-O2 cells) were cultured with DMEM (Dulbecco's modified Eagle medium) which contains supplement of 10% FBS (Fetal Bovine Serum). Human Dermal fibroblasts (HDFs) were cultured in DMEM Basic medium supplemented with 10% (v/v) bovine calf serum. All cell lines were cultured in a humidified incubator at 37 °C under 5% CO_2 atmosphere. Images were acquired using a confocal microscope (Zeiss LSM900).

2.4. Calculation of energy transfer efficiency (ETE)

ETE was calculated by following equation:

$$\eta_{ETE} = 1\text{-}F_{DA}/F_D$$

Where, F_{DA} and F_D denote the maximum of fluorescence intensity with and without an acceptor, respectively.

3. Results and discussion

3.1. Design of fluorescent probe NBIS

The energy transfer efficiency of FRET probes is highly dependent on the substantial overlap of the donor emission spectrum with the acceptor absorption spectrum. In addition, two well-separated emission bands with comparable intensities can ensure detection accuracy. However, because the larger the spectral overlap, the shorter the emission shifts of FRET systems, to reconcile the two parameters is difficult. Therefore, it is still a current challenge to construct new FRET pairs.

Naphthalimide derivatives are classical fluorophores and widely used to construct fluorescent probes including single emission or ratiometric signal. Due to the maximum emission of naphthalimide fluorophore is around 560 nm, it can be used as both donor and acceptor in the different FRET pairs, depending on the spectra of a second component [20,28,29,32]. Hemicyanine dyes are widely used in fluorescent probes based on ICT mechanism, because of its good solubility in water, high molar extinction coefficients and lower cell toxicity. As a part of ICT system, benzoindole moiety, generally in the cation form, due to the excellent electron-withdrawing ability, is often used [27,42–44]. According to the spectral property of hemicyanine dyes, they should be suitable as the acceptor for the construction of FRET platform. However, benzoindole-based hemicyanine dyes for FRET platform are still rare [45]. Therefore, in present work, a new FRET platform is constructed (named as **NBIS**), in which naphthalimide derivatives is selected as the donor and benzoindole-based hemicyanine is selected as the acceptor (Scheme 1). When probe **NBIS** in a buffer solution (DMSO/PBS = 3:7, pH = 7.4) was excited at 440 nm, the maximum emission centered 610 nm from acceptor moiety was observed because FRET process occurred. However, after the probe reacted with HSO_3^-/SO_3^{2-}, by a nucleophilic addition at C=C double bond in acceptor moiety, ICT process in the acceptor moiety was destroyed and FRET could no longer operate, leading to the donor emission at 534 nm was recorded. The visible light excitation (440 nm) and the spacing between two emission peaks (76 nm) could meet the requirements for the ratiometric detection.

3.2. Synthesis of probe **NBIS**

As shown in Scheme 2, compound **1** (1,1,2,3-tetramethyl-1*H*-benzo [*e*]indol-3-ium iodide) was easily synthesized from commercial 1,1,2-trimethyl-1*H*-benzo [*e*]indole by methylation with methyl iodide. Compound **1** condensed with 4-(piperazin-1-yl)benzaldehyde (**2**) to afford (*E*)-1,1,3-trimethyl-2-(4-(piperazin-1-yl)styryl)-1*H*-benzo [*e*] indol-3-ium iodide (compound **3**). The reaction of compound **4** and pyrrolidine gave 4-(1,3-dioxo-6-(pyrrolidin-1-yl)-1*H*-benzo [*de*]isoquinolin-2(3*H*)-yl)benzoic acid (compound **5**). Finally, compound **3** reacted with compound **5** to furnish probe **NBIS** (compound **6**), (*E*)-2-(4-(4-(4-(1,3-dioxo-6-(pyrrolidin-1-yl)-1*H*-benzo [*de*]isoquinolin-2(3*H*)-yl) benzoyl)piperazin-1-yl)styryl)-1,1,3-trimethyl-1*H*-benzo [*e*]indol-3-ium iodide.

3.3. Fluorescence and UV–Vis absorption spectral of probe **NBIS**

After a series of tests for a suitable solvent, a buffer solution (DMSO/PBS = 3:7, pH = 7.4) was chosen for all spectral property measurements. Probe **NBIS** alone in the buffer solution displayed a strong fluorescence band centered at 610 nm when it was excited with 440 nm light due to FRET process. The fluorescence quantum yield is $\Phi = 0.011$ (quinine sulfate as standard). The addition of HSO_3^-/SO_3^{2-} led to a new fluorescence band centered at 534 nm ($\Phi = 0.006$, quinine sulfate as standard). It can be observed that fluorescence intensity at 610 nm abated gradually and the fluorescence intensity at 534 nm increased as the dosage of HSO_3^-/SO_3^{2-} increased (Fig. 1 (a)). The phenomena fitted a typical FRET character. The fluorescence lifetime was measured and the results were shown in Fig. S5 and Table S1. The average fluorescence lifetime of donor moiety in the probe at 534 nm was shorter than that of the donor only, which confirmed the FRET process [46]. A preferable linearity between the fluorescence intensity ratios (I_{534}/I_{610}) and the concentrations of HSO_3^-/SO_3^{2-} from 0 to 0.9 equiv. Was obtained (Fig. 1 (b)). The limit of detection was calculated to be 16.2 nM, which is superior to previous reports (Table S2). The good sensitivity offers potential for the sensing of intracellular SO_2 derivatives. Similarly, the absorption spectrum showed that the absorbance at the longer wavelength decreased gradually and the absorbance in shorter wavelength changed little when added HSO_3^-/SO_3^{2-} in the range of 0–1.6 equiv. (Fig. S6). The addition reaction product of probe **NBIS** with HSO_3^-/SO_3^{2-} was verified by HRMS data (Fig. S7), in which the peak appeared at *m/z* 846.3257 was attributed to the addition product (calculated *m/z* $[M+H]^+$: 846.3320). Notably, the fluorescence emission spectrum of the donor could efficiently overlap with the absorption spectrum of the acceptor (Fig. S8). The energy transfer efficiency of the probe was calculated to be 89% (Fig. S9). Moreover, two emission peaks separated obviously with a 76 nm emission shift.

3.4. Selectivity of probe **NBIS** toward HSO_3^-/SO_3^{2-} by fluorescence spectrometry

The selectivity of a fluorescent probe toward analyte is one of the most important parameters. Therefore, the selectivity of probe **NBIS** toward HSO_3^-/SO_3^{2-} and other species (Cl^-, Br^-, I^-, AcO^-, NO_2^-, NO_3^-, SCN^-, $S_2O_3^{2-}$, HCO_3^-, SO_4^{2-}, HS^-, Cys, GSH, Hcy) was evaluated in the buffer solution. The fluorescence intensity ratio of the probe has few changes in the presence of Cl^-, Br^-, I^-, AcO^-, NO_2^-, NO_3^-, SCN^-, $S_2O_3^{2-}$, HCO_3^-, SO_4^{2-}, HS^-, Cys, GSH, Hcy, respectively. Moreover, the ratio (I_{534}/I_{610}) value dramatically increases 7.4-fold in the presence of HSO_3^-/SO_3^{2-}. The results indicate a high sensitivity of the probe toward HSO_3^-/SO_3^{2-} (Fig. S10). To appraise whether the probe can be preferable for the detection of HSO_3^-/SO_3^{2-} in the presence of other species (Cl^-, Br^-, I^-, AcO^-, NO_2^-, NO_3^-, SCN^-, $S_2O_3^{2-}$, HCO_3^-, SO_4^{2-}, HS^-, Cys, GSH, Hcy), the fluorescence spectra of the probe toward HSO_3^-/SO_3^{2-} (2 equiv.) in the presence of various species (2 equiv.), respectively, were measured and the fluorescence intensity ratios were almost not changed compared with that in the absence of other species (Fig. S10). Thus, probe **NBIS** showed high selectivity and good anti-interference ability for HSO_3^-/SO_3^{2-}, suggesting the applicability of the probe to detection of HSO_3^-/SO_3^{2-} in complex environments.

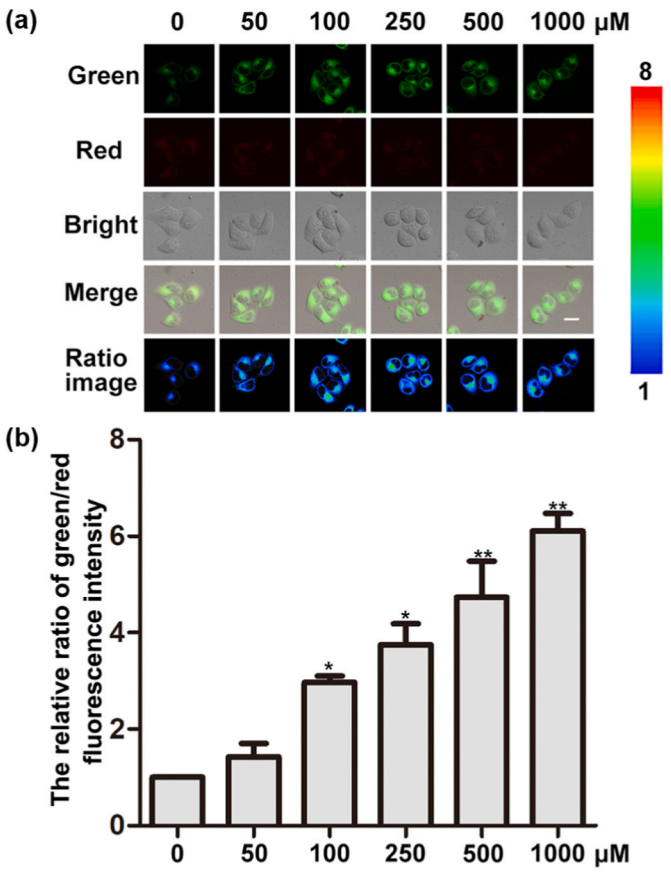

Fig. 2. Fluorescence and bright field images of exogenous HSO_3^-/SO_3^{2-} in HeLa cells. (a) HeLa cells were pre-incubated with probe **NBIS** (5 μM) for 1 h, followed by $NaHSO_3$ (0, 50, 100, 250, 500 and 1000 μM) for another 1 h. Scale bar: 20 μm. (b) The relative fluorescence intensity ratio of green/red. (λ_{ex} = 405 nm; green channel: 405–580 nm; red channel: 580–700 nm; data are presented as the mean ± SEM, *p < 0.05, **p < 0.01, n = 3).

3.5. Effect of pH and time on **NBIS** toward HSO_3^-/SO_3^{2-}

The properties of fluorescence probes depend strongly on solvent system and its pH because the reaction rate and equilibrium of nucleophilic addition is changed in the different solvent and pH. Therefore, in the condition of a selected solvent system, the effect of pH and time on **NBIS** toward HSO_3^-/SO_3^{2-} was determined. The fluorescence intensity ratios (I_{534}/I_{610}) of the probe was stable over a wide pH range (pH = 4–8). In addition, in the presence of HSO_3^-/SO_3^{2-}, the fluorescence intensity ratios (I_{534}/I_{610}) of the reaction solution increased with increases in pH from 5 to 7, however, no obvious change was observed in the range of pH 7–8 (Fig. S11), which should be suitable for bioimaging in living cells.

The response time of the probe toward HSO_3^-/SO_3^{2-} was recorded (Fig. S12). At room temperature, the reaction of the probe with HSO_3^-/SO_3^{2-} proceeded in the buffer solution leading to the fluorescence intensity ratios (I_{534}/I_{610}) gradually increasing and no longer change after 12 min. The response of the probe toward HSO_3^-/SO_3^{2-} was in the better category (Table S2), which could meet well the requirement of real-time detection.

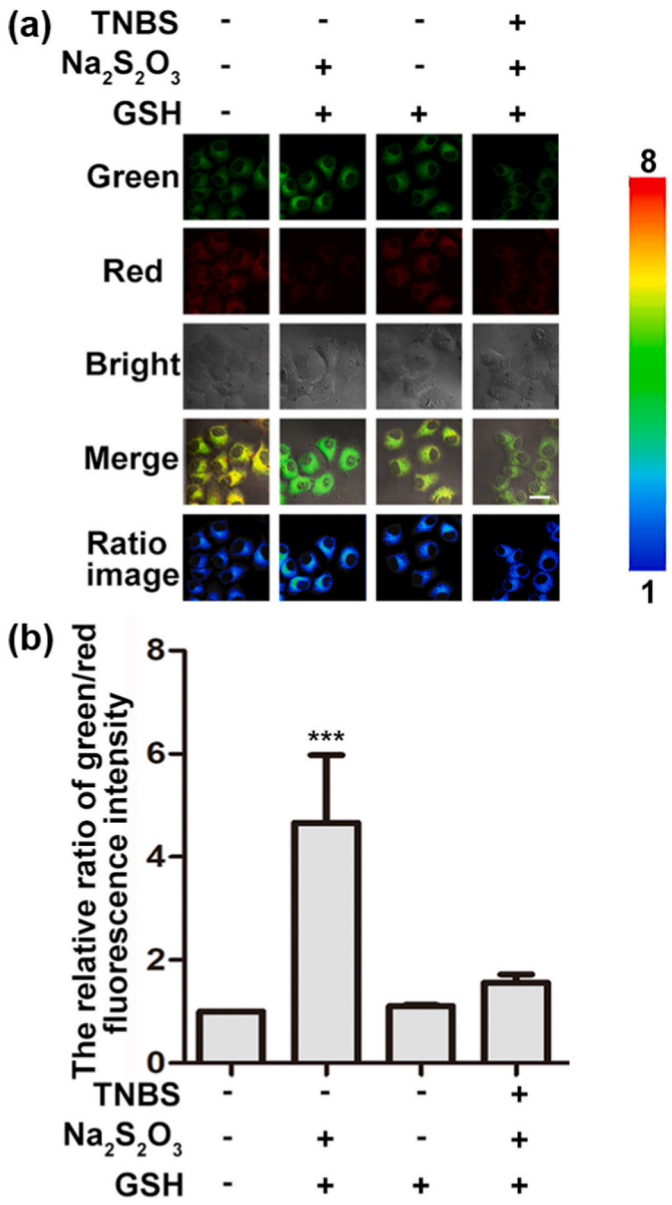

Fig. 3. (a) The first column: HepG2 cells were treated with probe **NBIS** (5 μM) for 1 h; The second column: HepG2 cells were pre-treated with GSH (500 μM) and $Na_2S_2O_3$ (250 μM) for 1 h before incubated with probe **NBIS** (5 μM) for another 1 h; The third column: HepG2 cells were pre-cultured with GSH (500 μM) for 1 h, and then cultured with probe **NBIS** (5 μM) for 1 h; The fourth column: HepG2 cells were treated for 1 h with GSH (500 μM) and $Na_2S_2O_3$ (250 μM) after pre-treatment with TNBS (10 mM) for 20 min, followed by probe **NBIS** (5 μM) for 1 h. Scale bar: 20 μm. (b) The fluorescence ratio of Green/Red of column 1, 2, 3 and 4 in (a). (λ_{ex} = 405 nm; green channel: 405–580 nm; red channel: 580–700 nm; data are presented as the mean ± SEM, ***p < 0.001, n = 3).

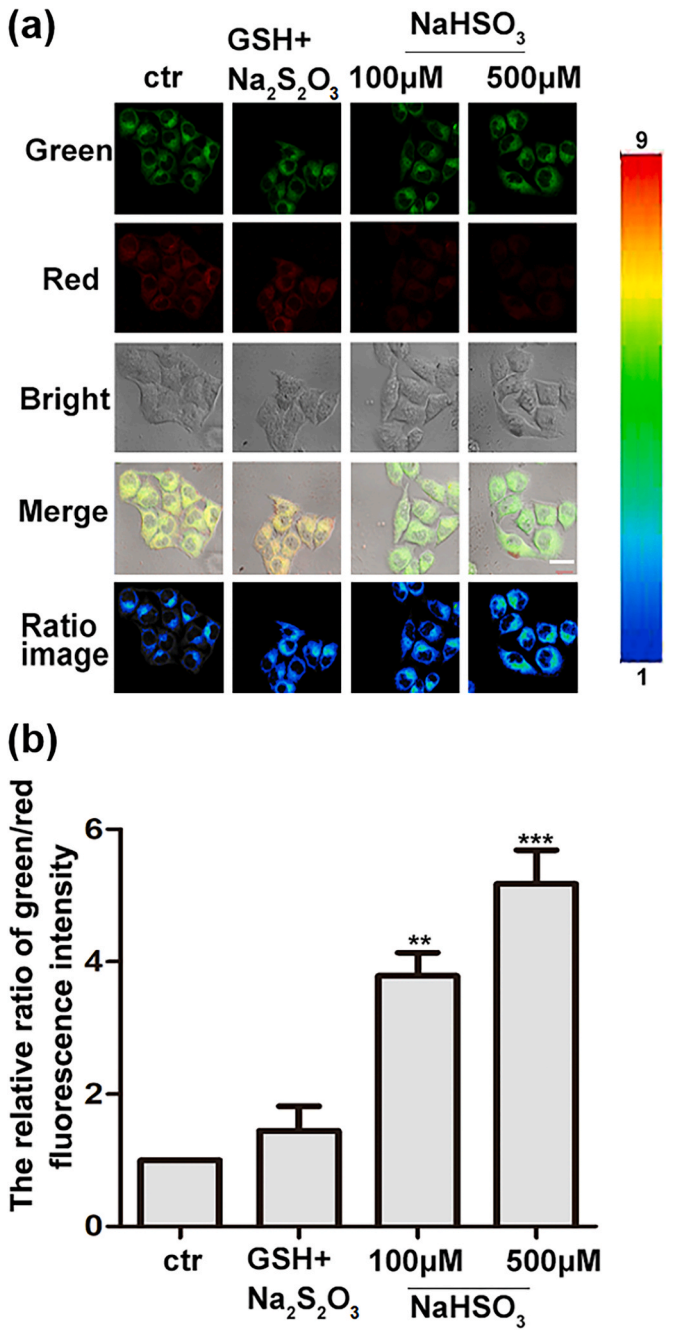

Fig. 4. (a) L-O2 cells were incubated with probe **NBIS** (5 μM) for 1 h, then with GSH (500 μM) and $Na_2S_2O_3$ (250 μM) or $NaHSO_3$ (100 and 500 μM) for another 1 h. (b) The relative ratio (Green/Red) of fluorescence intensity of column 1, 2, 3 and 4 in (a). Scale bar: 20 μm. (λ_{ex} = 405 nm; green channel: 405–580 nm; red channel: 580–700 nm; data are presented as the mean ± SEM, **p < 0.01, ***p < 0.001, n = 3).

3.6. Cell imaging of *NBIS*

After fluorescence properties of probe **NBIS** in the buffer solution for HSO_3^-/SO_3^{2-} was evaluated, the real-time detection of intracellular HSO_3^-/SO_3^{2-} was further achieved. According to SRB assay [47], the cytotoxicity of probe **NBIS** was primarily evaluated. The results revealed that the probe had no obvious cytotoxicity in HeLa cells (Fig. S13). The photostability of a probe in living cells is another crucial factor. Therefore, the photostability of probe **NBIS** in HeLa cells was put to the test, and the results revealed that the probe was photostable within 3 min (Fig. S14). The results showed that probe **NBIS** was suitable for bioimaging application.

The real time imaging of exogenous HSO_3^-/SO_3^{2-} in HeLa cells was investigated by the use of probe **NBIS.** HeLa cells were incubated with probe **NBIS** (5 μM) for 1 h and treated with exogenous HSO_3^-/SO_3^{2-} (0, 50, 100, 250, 500 and 1000 μM) respectively for 1 h. The imaging showed that the red fluorescence in 580–700 nm channel decreased gradually and the green fluorescence in 405–580 nm channel enhanced obviously as the increment of HSO_3^-/SO_3^{2-} (Fig. 2). The fluorescence intensity ratio (green/red) enlarged clearly along with the concentration increase of HSO_3^-/SO_3^{2-}, and even 6-fold enhancements (Fig. 2). Therefore, probe **NBIS** could realize real time and ratiometric detection

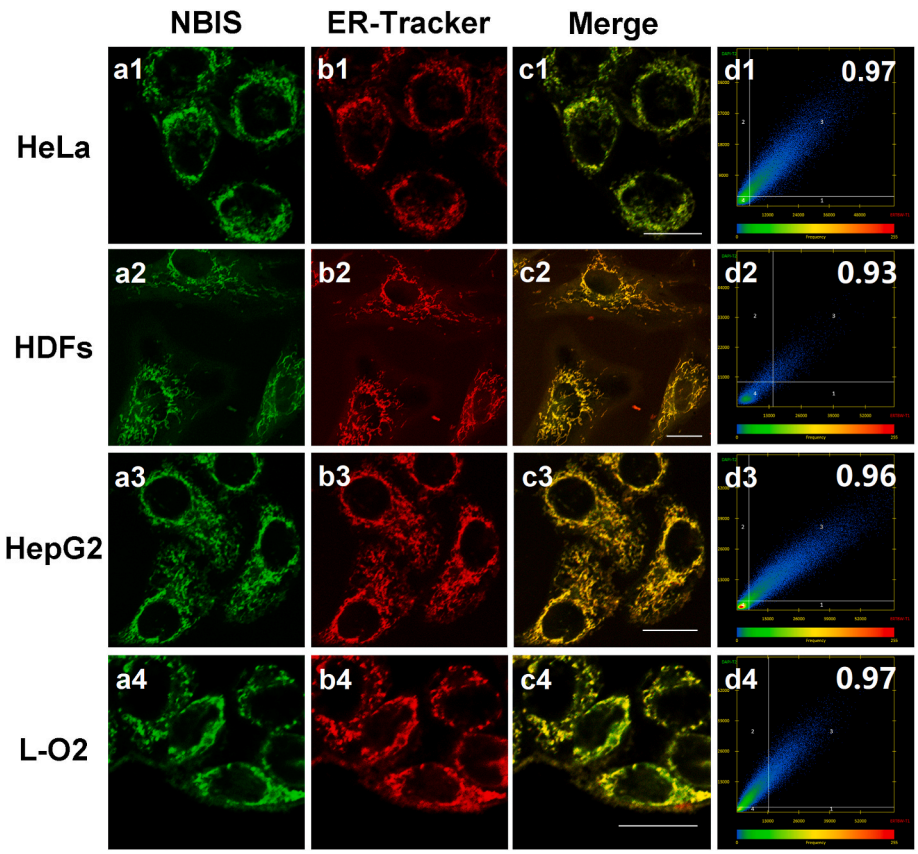

Fig. 5. HeLa cells, HDFs, HepG2 cells and L-O2 cells were incubated with probe **NBIS** (5 μM) for 1 h, afterward with ER-Tracker Red (1:200) for 30 min. a1-4: Fluorescence images of HeLa cells (a1), HDFs (a2), HepG2 cells (a3) and L-O2 cells (a4) with probe **NBIS** from the green channel (λ_{ex} = 405 nm; green channel: 405–580 nm). b1-4: Fluorescence images of HeLa cells (b1), HDFs (b2), HepG2 cells (b3) and L-O2 cells (b4) with ER-Tracker Red channel (λ_{ex} = 639 nm; red channel: 640–700 nm). c1-4: Merged images with (a1-4) and (b1-4). d1-4: Co-localization images of HeLa cells (d1) (MCC = 0.97), HDFs (d2) (MCC = 0.93), HepG2 cells (d3) (MCC = 0.96) and L-O2 cells (d4) (MCC = 0.97). Scale bar: 20 μm.

of HSO_3^-/SO_3^{2-} in living cells.

The ratiometric imaging of endogenous HSO_3^-/SO_3^{2-} in living HepG2 cells was fulfilled by probe **NBIS**. It is well known that endogenous SO_2 derivatives in mammalian liver cells could generate through thiosulfate sulfurtransferase (TST) catalyzed reaction of thiosulfate ($Na_2S_2O_3$) and glutathione (GSH). Thus, HepG2 cells were firstly pre-cultured with probe **NBIS** (5 μM) for 1 h, and incubated with GSH (500 μM) and $Na_2S_2O_3$ (250 μM) for 1 h, then confocal imaging was conducted. The results indicated that the cells showed an obvious bright green fluorescence and receded red fluorescence (Fig. 3 (a)). As a comparison, no obvious changes in the fluorescence of HepG2 cells loaded with probe **NBIS** and hatched with only GSH were observed. To further verify endogenous HSO_3^-/SO_3^{2-} in living HepG2 cells leading the changes in the fluorescence, 2,4,6-trinitrobenzenesulphonate (TNBS), a common inhibitor of the TST enzyme, was used. After HepG2 cells were hatched with TNBS (10 mM) for 20 min, followed by the treatment with GSH (500 μM) and $Na_2S_2O_3$ (250 μM) for 1 h, the cells were incubated with probe **NBIS** (5 μM) for 1 h. The imaging showed no clear fluorescence variation. Compared with other test groups, the relative ratio (green/red) of the fluorescence intensity of HepG2 cells treated with $Na_2S_2O_3$ and GSH exhibited clear variations and even 5-fold enhancements (Fig. 3 (b)). Therefore, probe **NBIS** could be successfully applied to image exogenous and endogenous HSO_3^-/SO_3^{2-} in living cells.

Our previous work illustrated that the concentration of the endogenous HSO_3^-/SO_3^{2-} was higher in liver cancer cells than that in normal liver cells [48,49]. In the present, for L-O2 cells loaded with probe **NBIS** and incubated with GSH and $Na_2S_2O_3$ for 1 h no obvious changes were recorded (Fig. 4). Therefore, the level difference of endogenous HSO_3^-/SO_3^{2-} from liver cancer cells and normal liver cells was further verified by probe **NBIS**.

Organelle-targeted fluorescent probes for bioactive species imaging are of great significance to research the biological roles of these molecules [41]. In this work, ER-targeted fluorescent probe **NBIS** for monitoring of HSO_3^-/SO_3^{2-} was discovered unexpectedly (Fig. 5). The endoplasmic reticulum (ER) is an important site for protein and lipid synthesis, calcium homeostasis and detoxification of poisonous substances [50]. It is reported that SO_2 preconditioning has a protective effect on rat myocardial ischemia/reperfusion injury and this process involves endoplasmic reticulum stress (ERS) [51]. SO_2 derivatives in liver tissue increased xanthine oxidase activity, induced ER stress and caused caspase activation [52]. Therefore, ER-targeted fluorescent probe **NBIS** could be useful for exploring physiological and pathological functions of SO_2 derivatives.

4. Conclusion

A new FRET-based fluorescent probe was constructed by the union of a naphthalimide fluorophore and a benzoindole-based hemicyanine fluorophore. The probe could detect HSO_3^-/SO_3^{2-} in ratiometric fluorescence manner with good selectivity and sensitivity. The probe could be excited by visible light and showed a satisfied energy transfer efficiency and clear spacing of two emission peaks. Moreover, the probe could target effectively the endoplasmic reticulum and was successfully used to image the endogenous and exogenous HSO_3^-/SO_3^{2-} in living cells.

Credit author statement

Zhang-Yi Li: Writing – original draft, Writing – review & editing, Synthesis and spectral property test of the probe. Xiao-Ling Cui: Cell imaging assay. Ye-Hao Yan: Spectral property test of the probe. Qiao-Ling Che: Synthesis of the probe. Jun-Ying Miao: Supervision. Bao-Xiang Zhao: Design of the probe, Supervision. Zhao-Min Lin: Cell imaging assay, Supervision.

Declaration of competing interest

The authors declare no conflicts of interest.

Acknowledgments

This study was supported by the National Key Research and Development Program of China (2017YFA0104604), the National Natural Science Foundation of China (No.31871407, 31741083, 31870831), the Natural Science Foundation of Shandong Province (ZR2018MB042). The authors acknowledge the assistance of Shandong University Structural Constituent and Physical Property Research Facilities.

Appendix A. Supplementary data

Supplementary data to this article can be found online at https://doi.org/10.1016/j.dyepig.2021.109180.

References

[1] Huang Y, Tang C, Du J, Jin H. Endogenous sulfur dioxide: a new member of gasotransmitter family in the cardiovascular system. Oxid. Med. Cell Longev. 2016: 8961951. https://doi.org/10.1155/2016/8961951. 2016.
[2] Song Y, Peng H, Bu D, Ding X, Yang F, Zhu Z, Tian X, Zhang L, Wang X, Tang C, Huang Y, Du J, Jin H. Negative auto-regulation of sulfur dioxide generation in vascular endothelial cells: AAT1 S-sulfenylation. Biochem Biophys Res Commun 2020;525:231–7. https://doi.org/10.1016/j.bbrc.2020.02.040.
[3] Pisoschi AM, Pop A, Gajaila I, Iordache F, Dobre R, Cazimir I, Serban A. Analytical methods applied to the assay of sulfur-containing preserving agents. Microchem J 2020;155:104681. https://doi.org/10.1016/j.microc.2020.104681.
[4] Yu W, Jin H, Tang C, Du J, Zhang Z. Sulfur-containing gaseous signal molecules, ion channels and cardiovascular diseases. Br J Pharmacol 2018;175:1114–25. https://doi.org/10.1111/bph.13829.
[5] Niu M, Han Y, Li Q, Zhang J. Endogenous sulfur dioxide regulates hippocampal neuron apoptosis in developing epileptic rats and is associated with the PERK signaling pathway. Neurosci Lett 2018;665:22–8. https://doi.org/10.1016/j.neulet.2017.11.036.
[6] Xu J, Yuan H, Zeng L, Bao G. Recent progress in Michael addition-based fluorescent probes for sulfur dioxide and its derivatives. Chin Chem Lett 2018;29:1456–64. https://doi.org/10.1016/j.cclet.2018.08.012.
[7] Li K, Li LL, Zhou Q, Yu KK, Kim JS, Yu XQ. Reaction-based fluorescent probes for SO_2 derivatives and their biological applications. Coord Chem Rev 2019;388: 310–33. https://doi.org/10.1016/j.ccr.2019.03.001.
[8] Yang B, Xu J, Zhu HL. Recent progress in the small-molecule fluorescent probes for the detection of sulfur dioxide derivatives (HSO_3^-/SO_3^{2-}). Free Radical Biol Med 2019;145:42–60. https://doi.org/10.1016/j.freeradbiomed.2019.09.007.
[9] Dong B, Song W, Lu Y, Kong X, Mehmood AH, Lin W. An ultrasensitive ratiometric fluorescent probe based on the ICT-PET-FRET mechanism for the quantitative measurement of pH values in the endoplasmic reticulum (ER). Chem Commun 2019;55:10776–9. https://doi.org/10.1039/C9CC03114F.
[10] Zhang Y, Xia S, Mikesell L, Whisman N, Fang M, Steenwinkel TE, Chen K, Luck RL, Werner T, Liu H. Near-infrared hybrid rhodol dyes with spiropyran switches for sensitive ratiometric sensing of pH changes in mitochondria and drosophila melanogaster first-instar larvae. ACS Appl. Bio Mater. 2019;2:4986–97. https://doi.org/10.1021/acsabm.9b00710.
[11] Lu X, Zhang G, Li D, Tian X, Ma W, Li S, Zhang Q, Zhou H, Wu J, Tian Y. Thiophene aromatic amine derivatives with two-photon activities as probes for the detection of picric acid and pH. Dyes Pigments 2019;170:107641. https://doi.org/10.1016/j.dyepig.2019.107641.
[12] Sun YQ, Liu J, Zhang J, Yang T, Guo W. Fluorescent probe for biological gas SO_2 derivatives bisulfite and sulfite. Chem Commun 2013;49:2637–9. https://doi.org/10.1039/C3CC39161B.
[13] Zhu L, Xu J, Sun Z, Fu B, Qin C, Zeng L, Hu X. A twisted intramolecular charge transfer probe for rapid and specific detection of trace biological SO_2 derivatives and bio-imaging applications. Chem Commun 2015;51:1154–6. https://doi.org/10.1039/C4CC08258C.
[14] Li H, Fan J, Long S, Du J, Wang J, Peng X. A fluorescent and colorimetric probe for imaging the mitochondrial sulfur dioxide in living cells. Sensor Actuator B Chem 2018;273:899–905. https://doi.org/10.1016/j.snb.2018.07.008.
[15] Zhao M, Liu D, Zhou L, Wu B, Tian X, Zhang Q, Zhou H, Yang J, Wu J, Tian Y. Two water-soluble two-photon fluorescence probes for ratiometric imaging endogenous SO_2 derivatives in mitochondria. Sensor Actuator B Chem 2018;255:1228–37. https://doi.org/10.1016/j.snb.2017.08.053.
[16] Tamima U, Santra M, Song CW, Reo YJ, Ahn KH. A benzopyronin-based two-photon fluorescent probe for ratiometric imaging of lysosomal bisulfite with complete spectral separation. Anal Chem 2019;91:10779–85. https://doi.org/10.1021/acs.analchem.9b02384.
[17] Lu Y, Li H, Yao Q, Sun W, Fan J, Du J, Wang J, Peng X. Lysozyme-targeted ratiometric fluorescent probe for SO_2 in living cells. Dyes Pigments 2020;180: 108440. https://doi.org/10.1016/j.dyepig.2020.108440.
[18] Samanta S, Halder S, Dey P, Manna U, Ramesh A, Das G. A ratiometric fluorogenic probe for the real-time detection of SO_3^{2-} in aqueous medium: application in a cellulose paper based device and potential to sense SO_3^{2-} in mitochondria. Analyst 2018;143:250–7. https://doi.org/10.1039/C7AN01368J.
[19] Xu W, Teoh CL, Peng J, Su D, Yuan L, Chang YT. A mitochondria-targeted ratiometric fluorescent probe to monitor endogenously generated sulfur dioxide derivatives in living cells. Biomaterials 2015;56:1–9. https://doi.org/10.1016/j.biomaterials.2015.03.038.
[20] Sun SG, Ding H, Yuan G, Zhou L. An efficient TP-FRET-based lysosome-targetable fluorescent probe for imaging peroxynitrite with two well-resolved emission channels in living cells, tissues and zebrafish. Anal Chim Acta 2020;1100:200–7. https://doi.org/10.1016/j.aca.2019.11.065.
[21] Xia S, Zhang Y, Fang M, Mikesell L, Steenwinkel TE, Wan S, Phillips T, Luck RL, Werner T, Liu H. A FRET-based near-infrared fluorescent probe for ratiometric detection of cysteine in mitochondria. ChemBioChem 2019;20:1986–94. https://doi.org/10.1002/cbic.201900071.
[22] Ren M, Wang L, Lv X, Sun Y, Chen H, Zhang K, Wu Q, Bai Y, Guo W. A rhodol-hemicyanine based ratiometric fluorescent probe for real-time monitoring of glutathione dynamics in living cells. Analyst 2019;144:7457–62. https://doi.org/10.1039/C9AN01852B.
[23] Tamima U, Song CW, Santra M, Reo YJ, Banna H, Islam MR, Ahn KH. A benzo[b]xanthene-derived fluorescent probe capable of two-photon ratiometric imaging of lysosomal cysteine with high specificity. Sensor Actuator B Chem 2020;322: 128588. https://doi.org/10.1016/j.snb.2020.128588.
[24] Hu Q, Qin C, Huang L, Wang H, Liu Q, Zeng L. Selective visualization of hypochlorite and its fluctuation in cancer cells by a mitochondria-targeting ratiometric fluorescent probe. Dyes Pigments 2018;149:253–60. https://doi.org/10.1016/j.dyepig.2017.10.002.
[25] Jun YW, Sarkar S, Singha S, Reo YJ, Kim HR, Kim JJ, Chang YT, Ahn KH. A two-photon fluorescent probe for ratiometric imaging of endogenous hypochlorous acid in live cells and tissues. Chem Commun 2017;53:10800–3. https://doi.org/10.1039/C7CC05834A.
[26] Gao J, He Y, Chen Y, Song D, Zhang Y, Qi F, Guo Z, He W. Reversible FRET fluorescent probe for ratiometric tracking of endogenous Fe^{3+} in ferroptosis. Inorg Chem 2020;59:10920–7. https://doi.org/10.1021/acs.inorgchem.0c01412.
[27] Roberts S, Seeger M, Jiang Y, Mishra A, Sigmund F, Stelzl A, Lauri A, Symvoulidis P, Rolbieski H, Preller M, Deán-Ben XL, Razansky D, Orschmann T, Desbordes SC, Vetschera P, Bach T, Ntziachristos V, Westmeyer GG. Calcium sensor for photoacoustic imaging. J Am Chem Soc 2018;140:2718–21. https://doi.org/10.1021/jacs.7b03064.
[28] Kong X, Li M, Dong B, Yin Y, Song W, Lin W. An ultrasensitivity fluorescent probe based on the ICT-FRET dual mechanisms for imaging β-galactosidase in vitro and ex vivo. Anal Chem 2019;91:15591–8. https://doi.org/10.1021/acs.analchem.9b03639.
[29] Zhang Y, Chen Y, Bai Y, Xue X, He W, Guo Z. FRET-based fluorescent ratiometric probes for the rapid detection of endogenous hydrogen sulphide in living cells. Analyst 2020;145:4233–8. https://doi.org/10.1039/D0AN00531B.
[30] Qian M, Zhang L, Pu Z, Xia J, Chen L, Xia Y, Cui H, Wang J, Peng X. A NIR fluorescent probe for the detection and visualization of hydrogen sulfide using the aldehyde group assisted thiolysis of dinitrophenyl ether strategy. J Mater Chem B 2018;6:7916–25. https://doi.org/10.1039/C8TB02218F.
[31] Zhang H, Wang B, Ye Y, Chen W, Song X. A ratiometric fluorescent probe for simultaneous detection of Cys/Hcy and GSH. Org Biomol Chem 2019;17:9631–5. https://doi.org/10.1039/C9OB01960J.
[32] Zhao X, Yuan G, Ding H, Zhou L, Lin Q. A TP-FRET-based fluorescent sensor for ratiometric visualization of selenocysteine derivatives in living cells, tissues and zebrafish. J Hazard Mater 2020;381:120918. https://doi.org/10.1016/j.jhazmat.2019.120918.
[33] Zhang W, Huo F, Cheng F, Yin C. Employing an ICT-FRET integration platform for the real-time tracking of SO_2 metabolism in cancer cells and tumor models. J Am Chem Soc 2020;142:6324–31. https://doi.org/10.1021/jacs.0c00992.
[34] Yan Y, Zhang X, Zhang X, Li N, Man H, Chen L, Xiao Y. Ratiometric sensing lysosomal pH in inflammatory macrophages by a BODIPY-rhodamine dyad with restrained FRET. Chin Chem Lett 2020;31:1091–4. https://doi.org/10.1016/j.cclet.2019.10.025.
[35] Jia X, Li W, Guo Z, Guo Z, Li Y, Zhang P, Wei C, Li X. An NBD-based mitochondrial targeting ratiometric fluorescent probe for hydrogen sulfide detection. Chemistry 2019;4:8671–5. https://doi.org/10.1002/slct.201901991.
[36] Zhang D, Liu A, Ji R, Dong J, Ge Y. A mitochondria-targeted and FRET-based ratiometric fluorescent probe for detection of SO_2 derivatives in water. Anal Chim Acta 2019;1055:133–9. https://doi.org/10.1016/j.aca.2018.12.042.
[37] Dong B, Tian M, Kong X, Song W, Lu Y, Lin W. Förster resonance energy transfer-based fluorescent probe for the selective imaging of hydroxylamine in living cells. Anal Chem 2019;91:11397–402. https://doi.org/10.1021/acs.analchem.9b02737.
[38] Wu WL, Wang ZY, Dai X, Miao JY, Zhao BX. An effective colorimetric and ratiometric fluorescent probe based FRET with a large Stokes shift for bisulfite. Sci Rep 2016;6:25315. https://doi.org/10.1038/srep25315.
[39] Wu WL, Ma HL, Huang MF, Miao JY, Zhao BX. Mitochondria-targeted ratiometric fluorescent probe based on FRET for bisulfite. Sensor Actuator B Chem 2017;241: 239–44. https://doi.org/10.1016/j.snb.2016.10.028.
[40] Li DP, Han XJ, Yan ZQ, Cui Y, Miao JY, Zhao BX. A far-red ratiometric fluorescent probe for SO_2 derivatives based on the ESIPT enhanced FRET platform with improved performance. Dyes Pigments 2018;151:95–101. https://doi.org/10.1016/j.dyepig.2017.12.056.

[41] Gao P, Pan W, Li N, Tang B. Fluorescent probes for organelle-targeted bioactive species imaging. Chem Sci 2019;10:6035–71. https://doi.org/10.1039/C9SC01652J.
[42] Zhu L, Fu M, Yin B, Wang L, Chen Y, Zhu Q. A red-emitting fluorescent probe for mitochondria-target microviscosity in living cells and blood viscosity detection in hyperglycemia mice. Dyes Pigments 2020;172:107859. https://doi.org/10.1016/j.dyepig.2019.107859.
[43] Zhao X, He F, Dai Y, Ma F, Qi Z. A single fluorescent probe for one- and two-photon imaging hydrogen sulfide and hydrogen polysulfides with different fluorescence signals. Dyes Pigments 2020;172:107818. https://doi.org/10.1016/j.dyepig.2019.107818.
[44] Chen B, Li C, Zhang J, Kan J, Jiang T, Zhou J, Ma H. Sensing and imaging of mitochondrial viscosity in living cells using a red fluorescent probe with a long lifetime. Chem Commun 2019;55:7410–3. https://doi.org/10.1039/C9CC03977E.
[45] Yan YH, Wu QR, Che QL, Ding MM, Xu M, Miao JY, Zhao BX, Lin ZM. A mitochondria-targeted fluorescent probe for the detection of endogenous SO_2 derivatives in living cells. Analyst 2020;145:2937–44. https://doi.org/10.1039/D0AN00086H.
[46] Clegg RM. Förster resonance energy transfer—FRET what is it, why do it, and how it's done. In: Laboratory techniques in biochemistry and molecular biology. Elsevier; 2009. p. 1–57. https://doi.org/10.1016/S0075-7535(08)00001-6.
[47] Skehan P, Storeng R, Scudiero D, Monks A, McMahon J. New colorimetric cytotoxicity assay for anticancer-drug screening. J Natl Cancer Inst 1990;82:1107–12. https://doi.org/10.1093/jnci/82.13.1107.
[48] Yan YH, Cui XL, Li ZY, Ding MM, Che QL, Miao JY, Zhao BX, Lin ZM. A synergetic FRET/ICT platform-based fluorescence probe for ratiometric imaging of bisulfite in lipid droplets. Anal Chim Acta 2020;1137:47–55. https://doi.org/10.1016/j.aca.2020.09.002.
[49] Li DP, Wang ZY, Cao XJ, Cui J, Wang X, Cui HZ, Miao JY, Zhao BX. A mitochondria-targeted fluorescent probe for ratiometric detection of endogenous sulfur dioxide derivatives in cancer cells. Chem Commun 2016;52:2760–3. https://doi.org/10.1039/C5CC09092J.
[50] Sitia R, Braakman I. Quality control in the endoplasmic reticulum protein factory. Nature 2003;426:891–4. https://doi.org/10.1038/nature02262.
[51] Wang XB, Huang XM, Ochs T, Li XY, Jin HF, Tang CS, Du JB. Effect of sulfur dioxide preconditioning on rat myocardial ischemia/reperfusion injury by inducing endoplasmic reticulum stress. Basic Res Cardiol 2011;106:865. https://doi.org/10.1007/s00395-011-0176-x.
[52] Ercan S, Kencebay C, Basaranlar G, Derin N, Aslan M. Induction of xanthine oxidase activity, endoplasmic reticulum stress and caspase activation by sodium metabisulfite in rat liver and their attenuation by Ghrelin. Food Chem Toxicol 2015;76:27–32. https://doi.org/10.1016/j.fct.2014.11.021.